Thermal conductivity and thermal cyclic fatigue of multilayered $Gd_2Zr_2O_7$/YSZ thermal barrier coatings processed by suspension plasma spray

Satyapal Mahade, Nicholas Curry, Stefan Björklund, Nicolaie Markocsan, Per Nylén

PII: S0257-8972(15)30383-2
DOI: doi: 10.1016/j.surfcoat.2015.11.009
Reference: SCT 20706

To appear in: *Surface & Coatings Technology*

Received date: 10 July 2015
Revised date: 2 November 2015
Accepted date: 6 November 2015

Please cite this article as: Satyapal Mahade, Nicholas Curry, Stefan Björklund, Nicolaie Markocsan, Per Nylén, Thermal conductivity and thermal cyclic fatigue of multilayered $Gd_2Zr_2O_7$/YSZ thermal barrier coatings processed by suspension plasma spray, *Surface & Coatings Technology* (2015), doi: 10.1016/j.surfcoat.2015.11.009

Thermal Conductivity and Thermal Cyclic Fatigue of Multilayered $Gd_2Zr_2O_7$/YSZ Thermal Barrier Coatings Processed by Suspension Plasma Spray

Satyapal Mahade[1*], Nicholas Curry[2], Stefan Björklund[1], Nicolaie Markocsan[1], Per Nylén[1]

[1] Department of Engineering Science, University West, Sweden

[2] Treibacher Industrie AG, Austria

Abstract

Rare earth zirconates have lower thermal conductivity, better phase stability, improved sintering resistance & CMAS (calcium magnesium alumino silicates) infiltration resistance than yttria stabilized zirconia (YSZ) at temperatures above 1200°C. However, their lower fracture toughness & lower coefficient of thermal expansion (CTE) compared to YSZ leads to premature coating failure. In order to overcome these drawbacks at higher temperatures, a multilayered coating approach is attempted in this study and compared with the single layer YSZ. Suspension plasma spray of single layer YSZ, single layer gadolinium zirconate (GZ) and double layer GZ/YSZ was carried out. Additionally, a triple layer coating system, with denser gadolinium zirconate on top of the GZ/YSZ system was sprayed to impart an added functionality of sealing the TBC from CMAS infiltration. Microstructural analysis was done using scanning electron microscopy and optical microscopy. Columnar microstructure with vertical cracks was observed. XRD analysis was used to identify phases formed in the as sprayed TBC samples. Porosity measurements were done using water impregnation method. Thermal diffusivity of single and multi-layered coatings was obtained by laser flash analysis and thermal conductivity of the coating systems was determined. It was found that the thermal conductivity of single layer gadolinium zirconate was lower than YSZ and thermal conductivity of multilayered systems were between their respective single layers. Theoretical thermal conductivity of the double layered (GZ/YSZ) system was also calculated using the rule of mixtures. The single (YSZ), double (GZ/YSZ) and triple (GZ dense/GZ/YSZ) layer TBCs were subjected to thermal cyclic fatigue (TCF) test at 1100°C & 1200°C. It was observed that the single layer YSZ had lowest TCF life whereas the triple layer TBC had highest TCF life irrespective of test temperature.

Keywords:

Gadolinium Zirconate, Multilayered Thermal barrier coating, Suspension Plasma Spray, Thermal Conductivity, Thermal Cyclic Fatigue, Thermal Diffusivity, Yttria Stabilized Zirconia

Corresponding Author

Satyapal Mahade, Email: satyapal.mahade@hv.se or satyapal14@gmail.com

PhD student, Production Technology Center, University West, Sweden

1. Introduction:

Thermal barrier coatings (TBC) are applied on the metallic components used in gas turbine engines in order to protect them from being exposed to high temperatures. Current market need of the gas turbine industry is to achieve higher efficiency in order to improve the fuel economy and lower harmful emissions. Such an increase in efficiency of gas turbines can be achieved by increasing the combustion temperature [1-3]. Higher combustion temperatures (>1200°C) pose severe challenges to the TBCs such as sintering, phase instability, oxidation, and CMAS (Calcium Magnesium Alumino Silicates) infiltration. Yttria stabilized zirconia (YSZ) is the standard top coat material used in thermal barrier coatings. But it undergoes significant sintering above 1200°C, which is not desirable [4]. Furthermore, YSZ is susceptible to CMAS infiltration, which results in loss of strain tolerance and change in near surface mechanical properties leading to early coating spallation [5-13].

Due to the drawbacks of YSZ above 1200°C, the search for new TBC materials for high temperature applications without compromising the preliminary requirements such as sintering resistance, excellent phase stability, lower thermal conductivity, higher coefficient of thermal expansion, good oxidation resistance, and CMAS penetration resistance is desirable. Pyrochlores are promising TBC topcoat candidates which can fulfill these requirements at higher temperatures [14-19]. Among the pyrochlores, gadolinium zirconate ($Gd_2Zr_2O_7$) is an interesting choice as lanthanum zirconate is difficult to process due to the tendency of La_2O_3 to evaporate and result in loss of desired stoichiometry [20-22]. Gadolinium zirconate (GZ) has excellent phase stability and lower bulk thermal conductivity than YSZ. However, it has a lower fracture toughness [23-25] and also GZ has a tendency to react and degrade alumina that forms the protective thermally grown oxide (TGO) above 1200°C [26]. In order to overcome these drawbacks, a multilayered approach with GZ on top of YSZ is in use to enhance the lifetime of TBC [27-29].

Conventional thermally sprayed TBC ceramics are processed by APS (Atmospheric Plasma Spray). The preferable particle size of the feedstock used in APS ranges from 10-140 µm. It was found that with the use of nano sized powders, improvement in thermal shock resistance can be obtained due to the lower tensile stress in plane and higher fracture toughness of nanostructured layers [30-32]. However, feeding of powders below 10µm into a plasma jet is considered near impossible and agglomerated nano powders retain only a little of their original structure in the final coating [33-34].

Suspension plasma spray (SPS) is a development of the APS process that makes it possible to use nano or submicron sized powders suspended in a solvent that acts as a carrier [35]. In particular, the recent developments of columnar-type coatings that mimic Electron Beam-Physical Vapor Deposition coatings have shown great promise as new TBC coatings [36-39].

To the best of author's knowledge, so far no literature is reported on the suspension plasma spray of GZ/YSZ multilayered TBC's and also very limited work is seen on evaluation of thermal conductivity of multilayered ceramic systems. The main objective of this study was to design high temperature resistant TBC system by suspension plasma spray process and for this purpose a double layer GZ/YSZ approach was chosen. Also, for CMAS protection, a triple layer system with denser sealing layer on top was investigated. The multilayered coatings are characterized for microstructure, phase analysis, porosity content, thermal diffusivity, thermal conductivity and thermal cyclic fatigue life. Single layer YSZ & single

layer GZ were also sprayed and compared with the multilayered systems for thermal cyclic fatigue and thermal conductivity respectively.

2. Experimental Method

2.1 Substrate and Bond Coat Preparation

Hastelloy-X substrates of 25mm x 25 mm x 1.54mm (square plates), 50mm x 30 mm x 6mm (thermal cyclic fatigue [TCF] plates) and 25.4 mm x 6.35 mm dimensions were grit blasted with alumina particles of 220 grit size to create a desired surface roughness R_a profile of 3 µm. The recently developed high velocity air fuel (HVAF) process was used to deposit NiCoCrAlY composition (AMDRY 9951, Oerlikon Metco, Switzerland) bondcoat of 220 µm thickness using M3 (Uniquecoat; Richmond, USA) gun on all the grit blasted substrates. Surface roughness of the as sprayed bondcoat was measured to be approximately 5 µm on R_a scale. Bond coat thickness (220 µm) on all the substrates was kept the same.

2.2 Suspension Plasma Spray Parameters

For this study, two suspensions were produced by Treibacher Industrie AG (Althofen, Austria). The first was an 8YSZ suspension with a median particle size of D_{50} = 500 nm dispersed in ethanol with a solid content of 25 wt%. The second suspension was gadolinium zirconate of the same particle size (D_{50} = 500 nm), suspended in ethanol with a solid content of 25 wt %.

Suspensions were sprayed using an Axial III plasma gun and Nanofeed 350 suspension feeding system (Northwest Mettech Corp., North Vancouver, Canada). A 3/8 inch plasma exit nozzle was utilized with internal axial injection of suspension via a 250µm diameter orifice. In all cases the suspension was fed at a rate of 45ml/min. Spray parameters for the coatings are shown in Table I. Two different parameters were selected for coating production with the first designed to produce columnar coatings. The second parameter was designed for production of denser coatings by virtue of being hotter (higher enthalpy) and slower (lower total gas flow) than the columnar parameter. Additionally the atomization gas flow to the axial injector was reduced. Overall the process changes have the effect of increasing the overall size of the atomized suspension droplets due to decreased plasma velocity [39]. According to the understood theory of SPS coating deposition, larger droplets will lead to more continuous or dense coatings rather than columnar coatings [36, 39].

Three variations in the ceramic coating structure were produced according to the schematic shown in Fig. 1. The first variation comprised of a single layer columnar coating of YSZ with a thickness of 300 µm. The second variation was a dual-layered columnar ceramic coating comprising of GZ (260 µm thick) as the top coat on YSZ base layer (60 µm thick). The total thickness of the double layered ceramic coat (GZ/YSZ) was approximately 320 µm. The third variation was a three layered ceramic coat comprising of a denser GZ (sealing layer for CMAS) on top of the dual-layer, columnar GZ/YSZ system. The thickness of the denser GZ was approximately 30 µm, whereas the thickness of relatively porous gadolinium zirconate & YSZ lying beneath was 230 µm & 60 µm respectively. The spray parameter for the dense layer was modified in order to achieve a dense microstructure rather than the porous, columnar structure desired for the other layers in the coating system. Additionally, a single layer GZ was also sprayed using the same set of spray parameters as that for the single layer YSZ for thermal conductivity measurement.

2.3 Coating Characterization

2.3.1 Metallography & Microstructure

In order to analyze the cross section of as sprayed TBC samples, sectioning was carried out using a slow speed diamond cutting blade and then later cold mounted by a 5:1 combination of epoxy resin & hardener. Polishing was carried out on 220 grit, 140 grit size discs successively and then with diamond paste of 9 micron, 6 micron, 3 micron respectively. Final polishing step was carried out on 0.05 micron silica paste until a scratch free mirror finished surface was obtained. Thickness measurements from 15 different locations of the coating cross section were done by optical microscopy and the average thickness value of each layer was determined. Scanning electron microscope (TM 3000, HITACHI, Japan) in back scattered electron (BSE) mode was used to observe the cross section and top view of the sprayed ceramic layers.

2.3.1.1 Column density & Column width measurement

A horizontal straight line of fixed length passing through half of the coating thickness was drawn on the cross sectional SEM micrographs at 300X magnification and all the columns gaps intercepting the line were considered. The column density was calculated using Eq. (1). A total of 25 micrographs of same magnification were considered for the column density measurements and the average values for each variation is reported.

$$Column\ density\ (\frac{Columns}{mm}) = \frac{No.\ of\ column\ gaps\ intercepted\ by\ the\ line}{True\ length\ of\ the\ line} \quad \textbf{(1)}$$

Also, the distance between two column gaps, which is known as the 'column width', was calculated from the same 25 cross sectional SEM micrographs used for column density measurements and the average column width is reported.

2.3.2 Porosity Measurements

Porosity content of the as sprayed TBC samples was analyzed by water impregnation method. In this method, free standing coatings were produced by dipping the TBC samples in a solution containing nitric acid and hydrochloric acid in 1:3 volume ratio for a time period of 1 hour. The samples were washed with water and dried in an oven, after which the dry weight of free standing coatings was measured. Later on, the free standing coatings were impregnated with water in a vacuum chamber and vacuumed several times to allow water to infiltrate the pores of coating. Wet weight of the coatings was measured and the difference between dry and wet weight was calculated. The densities of ceramic and water was known and the weight of the water and coating was also known. The total volume fraction of porosity content (P) was calculated. Bulk densities (ρ_b) of gadolinium zirconate, YSZ and GZ/YSZ multilayered systems are 6.32, 6.1 & 6.27 g/cm^3 respectively and the actual densities (ρ_a) of as sprayed coatings after taking into account the obtained porosity value were calculated according to Eq. (2).

$$\rho_a = \rho_b(1 - P) \quad \textbf{(2)}$$

2.3.2.1 Image Analysis

Porosity content of the as sprayed coatings was also measured by Image J, image analysis software [40]. SEM micrographs of 1500X magnification were chosen to capture finer pores

and also to ensure better contrast between pores and the ceramic. Twenty five different SEM micrographs of same magnification were used to evaluate the porosity and their mean values along with standard deviations were obtained. Column gaps in the microstructure were not considered for the porosity measurements by this method.

2.3.3 Thermal Diffusivity & Conductivity Measurements

Thermal diffusivity measurements were made using a NETZSCH 427 laser flash analysis (LFA) equipment (Netzsch Thermophysics, Selb, Germany). All measurements were performed under an argon environment. TBC samples of 10 mm diameter were water jet cut from square plates (25 mm X 25 mm x 1.54 mm) and gold sputtered (approximately 500nm thick) in order to prevent the direct transmission of infra-red light though the ceramic layer and also to improve the energy transfer to the sample. A thin layer of graphite is also coated in order to impart better absorption and emission properties. During the diffusivity measurements, rear surface of the 10mm diameter sample was exposed to a laser of known pulse width and the infra-red detector placed above the front face of sample recorded the rise in temperature.

$$\alpha = \frac{(0.1388 \times d^2)}{t_{0.5}} \quad \textbf{(3)}$$

Thermal diffusivity values were obtained according to the Eq. (3), where 'α' is the thermal diffusivity (mm^2/s), 'd' is the coating thickness (mm) and '$t_{0.5}$' is the half time taken for rise in temperature measured by the LFA equipment. The analysis was performed using a Cowan three layer model (substrate + bond coat + ceramic) with pulse correction. In this model, only the diffusivity of ceramic layer is the unknown and the thermal diffusivity, specific heat, density and thickness of the other two layers (substrate & bond coat) were measured in previous experiments. Also, the thermal contact resistance between each layer was measured before calculating the diffusivity of the unknown ceramic layer.

Specific heat capacity measurements were made using the NETZSCH 404 DSC equipment (Netzsch Thermophysics, Selb, Germany) utilizing ceramic powders obtained from crushing free standing coatings. Sapphire was used as the reference and C_p ratio method was used to evaluate the specific heat capacity in the range of 25°C to 1000°C.

Thermal conductivity of the as sprayed coatings was calculated according to Eq. (4), where 'λ' is the thermal conductivity, 'α' is the obtained thermal diffusivity, Cp is the obtained specific heat capacity and 'ρ' is the coating density. The accuracy of thermal conductivity calculation depends on the accuracy in measurement of the three variables on the right hand side of Eq. (4).

$$\lambda = \alpha(T).C_p(T).\rho \quad \textbf{(4)}$$

2.3.4 Phase Analysis

X Ray Diffraction (XRD) analysis of the as sprayed coatings was done using SEIFERT TT 3003 equipment to examine the various phases present in the top coat. Cu K_α of 1.541 A° wavelength was used. Slow scan rate with a step size of 0.01° and time per step of 10 s was used.

2.3.5 Thermal Cyclic Fatigue

TCF testing was carried out at 1100°C & 1200°C in a specially designed computer controlled furnace with a periodic quenching capability. It comprises of two chambers. In the first chamber, the TCF test plates are heated to 1100°C for a time period of 1 hour. Samples are then moved to the second chamber where photographs are captured by a high resolution camera and the samples are cooled down to 25°C in 10 minutes by compressed air. The samples are subjected to thermal cycling until a visible 20% spallation of the top ceramic layer is observed. Three samples from each variation of as sprayed TBCs were considered for the test. The failed TCF plates were cold mounted in epoxy resin, prepared as described previously and then analyzed by SEM.

3. Results & Discussion

3.1 Microstructural Analysis

The cross sectional SEM micrograph of as sprayed single layer YSZ, as seen in Fig. 2(a), shows a columnar microstructure with evenly distributed pores and the top view microstructure in Fig. 2(b) shows a cauliflower-like top surface structure. The average thickness of bond coat and the top YSZ layer were 220 µm and 300µm respectively. The average column density was found to be 12 ± 3 columns/mm and the average column width was 64 ± 10 µm.

The double layer GZ/YSZ microstructure in Fig. 3(a) also displays a columnar microstructure and a cauliflower-like microstructure from the top, as seen in in Fig. 3(b). Columns within the GZ layer have continued to build on those first formed by the YSZ base layer due to almost identical deposition conditions. Also, at higher magnifications, the GZ/YSZ interface was continuous showing good bonding between the layers. The average thickness of bond coat, YSZ and the top gadolinium zirconate was 220µm, 60µm and 260µm respectively. The average column density was found to be 11 ± 2 columns/mm and the average column width was 70 ± 8 µm.

In the case of triple layered GZ (dense)/GZ/YSZ, the top denser gadolinium zirconate layer meant for CMAS penetration resistance does not build on the columns of underlying GZ/YSZ system, as seen in Fig. 4(a); but instead forms a layered structure. The number of spray passes for denser GZ layer can be easily seen from the coating cross section**.** The top view SEM micrograph, as seen in Fig. 4(b), showed cauliflower microstructure. The average column density of underlying GZ/YSZ was found to be 11 ± 2 columns/mm and the average column width was 68 ± 10 µm.

3.2 Thermal Diffusivity

Thermal diffusivity values obtained from the laser flash analysis equipment are plotted in Fig. 5. The thermal diffusivity of multilayered (double & triple) ceramic system was calculated by treating the entire ceramic system as a single unit. Single layer YSZ and single layer gadolinium zirconate were also investigated. In all the coating systems, five different measurements were made at each temperature (25, 200, 400, 600, 800 & 1000°C) and their arithmetic mean value along with the mean standard deviations were obtained. The error (precision) in thermal diffusivity measurements were in the order of 0.001 to 0.012 mm^2/s and the experimental uncertainty associated to accuracy in thermal diffusivity measurement by laser flash analysis is 2% (as claimed by the equipment manufacturers). Gauss law of error

propagation was used to estimate the overall error (precision & accuracy) in thermal diffusivity measurement.

Thermal diffusivity values of all the coatings tend to increase at about 900°C to 1000°C. This may be attributed to two possible factors. Firstly, at temperatures above 900°C, sintering of the ceramic structure begins to occur; causing an increase in thermal conductivity. Secondly, the radiative mode of heat transfer in ceramic coating begins to show a greater influence above 900°C. A similar trend in thermal diffusivity of APS sprayed YSZ & GZ was reported by Moskal et al [41] using the three layer (Substrate + Bond coat + Ceramic) thermal diffusivity model.

3.3 Porosity Measurement

3.3.1 Water Intrusion Method

Free standing coatings were used to measure the porosity content by water impregnation method. This method estimates only open porosity content of a coating system as water cannot infiltrate pores which are closed and isolated. Results of porosity content of different coating systems investigated in this study are plotted in Fig. 6. Single layer GZ had a higher porosity content of 22 % followed by the GZ/YSZ double layered system with 20.5% and triple layered system with 17.4% respectively. Single layered YSZ coating had the lowest porosity content of 17%. The porosity values of double and triple layered systems lie in between their respective single layers, which was as expected. Also, the triple layer had almost 15 % lower porosity relative to the double layer system due to the presence of a denser top layer. If the porosity of double layer GZ/YSZ coating was estimated by weighed average (thickness proportions) using the porosity value of the single layer systems; then the value would have been 21.04%, which is slightly higher than the estimated value of 20.5% obtained by water intrusion method but in good agreement with the results.

3.3.2 Image Analysis Method

Porosity values & ranking of the as sprayed TBCs estimated by image analysis at 1500X are different from the values & ranking obtained by water intrusion method, as seen in Fig. 6. The reason could be due to the presence of higher number of closed pores in the case of YSZ than GZ which cannot be detected by water intrusion method. Image analysis can estimate the total porosity of a coating provided the image resolution is sufficiently high to identify the smallest scale pores. However, this software does not consider column gaps or vertical cracks into account as it is difficult to capture them at higher magnification. These column gaps make a significant contribution towards the total porosity content of a coating which is estimated by water intrusion method and hence explains the higher porosity value compared to image analysis. Additionally, image analysis helps in measuring porosity of each individual layer of a multilayered coating. The individual porosity contribution of denser GZ sealing layer in the case of triple layered TBC was found to be approximately 6.8% by image analysis.

3.4 Thermal conductivity

Thermal conductivity of the different coating systems was calculated according to Eq. (4) using experimentally obtained thermal diffusivity, specific heat capacity and density values. The error in thermal conductivity measurement in the temperature range of 25ºC to 1000ºC was calculated as per law of error propagation principle after taking into account the

experimental uncertainty (accuracy & precision) associated while measuring specific heat capacity, density & thermal diffusivity of the coatings. Porosity values estimated by water intrusion method were used for the density calculation for the sake of simplicity. The thermal conductivity values of single layer YSZ, single layer GZ, double layer GZ/YSZ and triple layer GZ (dense)/GZ/YSZ along with error in measurement are plotted in Fig. 7.

Thermal conductivity of YSZ obtained in this work was similar to the trend reported by Pawlosky et al [42] & Curry et al [37, 43] on suspension plasma sprayed YSZ coatings. In the case of standard APS sprayed YSZ, thermal conductivity decreases with increase in temperature up to 800ºC and then begins to increase due to sintering effects. However, in SPS sprayed YSZ, the thermal conductivity increases with temperature, as shown in Fig. 7. In SPS coatings, the presence of fine scale microstructural features, which include fine scale porosity & fine grains, contribute to multiple interfaces. These imperfections within the coating can affect the mean free path of phonons and eventually affect the thermal conductivity of the coating. Single layer GZ had a lower thermal conductivity compared to single layer YSZ, as seen in Fig. 7, in the temperature range of 25 to 1000°C due to the lower thermal diffusivity & lower specific heat capacity of GZ than YSZ [18]. SPS sprayed GZ had a lower thermal conductivity (absolute value) compared to APS sprayed GZ but their trend was similar as reported by Moskal et al [41]. Thermal conductivity values of the double and triple layered TBCs lie in between the thermal conductivities of single layer YSZ & single layer GZ.

3.5 XRD Analysis

The XRD profiles of as sprayed single layer (YSZ), double layer (GZ/YSZ) & triple layer (GZ (dense)/GZ/YSZ) are plotted in Fig. 8. The peaks were identified by JCPDS standard and labelled. The obtained XRD profiles indicate that double and triple layered systems have peaks at same positions (angles) indicating the presence of same composition ($Gd_2Zr_2O_7$) and crystal structure (cubic) irrespective of spray parameters. Additionally, it also confirms that there is no change in the stoichiometry during GZ spraying. Loss in stoichiometry of the ceramic while spraying may lead to degradation in thermo chemical (CMAS resistance) & thermo mechanical (TCF life) properties of the coating. In the case of YSZ, tetragonal (t') phase of ZrO_2 with no presence of monoclinic phase was observed. Monoclinic phase of ZrO_2 is not desirable in the as sprayed TBC as it undergoes phase transformation during thermal cycling, leading to large volume changes which causes premature coating spallation.

3.6 Thermo Cyclic Fatigue test

Results of thermal cyclic fatigue (TCF) at 1100°C are shown in Fig. 9. Single layer YSZ had the lowest TCF life whereas the double layer GZ/YSZ system was better than single layer YSZ system by approximately 40 cycles. The reason for improvement in thermal cyclic fatigue life of double layer system may be attributed towards the better oxygen penetration resistance of pyrochlores than YSZ [44-45]. This is due to the presence of vacant '48f' position and an interstitial oxygen anion at '8b' position in the crystal structure of pyrochlores which together constitute a stable oxygen anion frenkel pair [46-50]. Also, atomistic simulation studies showed that rare earth zirconates (pyrochlores) have higher oxygen anion frenkel pair energy and therefore it requires higher activation energy for oxygen migration [51-52]. Further improvement in thermal cyclic life of up to 28 cycles compared to the double layer was observed in the triple layered GZ (dense)/GZ/YSZ. The reason for improvement in TCF life is probably due to the presence of a 30 micron thick denser gadolinium zirconate

layer on top of the 230 micron gadolinium zirconate layer and 60 micron YSZ. It is an established fact in TBCs that oxygen gains access to the bond coat of a TBC system through vacancies in the ceramic crystal structure and porosity in the coating. The denser gadolinium layer helps in further reducing oxygen penetration into the coating system due to almost 15 % lower porosity content (according to water intrusion results) than the double layer TBC. A similar trend of triple layer TBC outperforming the double and single layer TBC was observed in TCF test at 1200°C, as seen in Fig. 9. However the cyclic fatigue life decreased drastically due to the severity of temperature and absence of thermal gradient across the cross section of TCF sample.

The photographs & SEM micrographs of the failed samples after TCF testing at 1100°C are shown in Fig. 10, 11 &12**.** The failed photograph of triple layer TBC, Fig. 12(b), was taken well beyond its reported lifetime as the failure occurred in the absence of manual inspection. But the lifetime is calculated at 20 % coating spallation by looking at the images captured by high resolution camera after each cycle. SEM micrograph of TCF failed single layer YSZ in Fig. 10(a) showed that spallation occurred at the bond coat and YSZ interface, which is the common mode of failure observed in suspension plasma sprayed coatings [37-39].

Failure in the GZ/YSZ double layer TBC, as seen in Fig. 11(a) & (b), occurred in GZ layer very near to the interface with YSZ layer. Reason for such a failure may be due to the CTE mismatch between the GZ & YSZ. Also, GZ exhibits a lower fracture toughness compared to YSZ which leads to crack propagation at lower stress levels in the GZ layer. Similar cracking was reported previously for YSZ stabilized in the cubic phase, potentially due to its reduced fracture toughness [39].

In the case of TCF failed triple layer TBC, as seen in Fig. 12(a), failure occurred at the bond coat & YSZ interface. Higher enthalpy & higher power was used to deposit the denser GZ layer in triple layer TBC, according to Table I. Reason for a different TCF failure mode compared to GZ/YSZ double layer TBC could be due to release of fraction of energy stored in the coating in the form of horizontal crack propagation at the interface of GZ dense & GZ layer, as seen in Fig. 12(a). Average TGO thickness was calculated from the failed TBC SEM micrographs at higher magnifications and it was found that all the three TBCs had a TGO thickness of approximately 5 µm. The TGO thickness at failure in SPS coatings obtained is in close agreement with literature reported on failure of APS sprayed YSZ, where 6-7 µm thick TGO was observed in the TCF test [53].

Conclusions

Suspension plasma spray of multilayered (double & triple layer) TBCs was carried out and their functional performance (thermal conductivity & thermal cyclic fatigue) was compared with the current standard YSZ single layer TBC. It was shown that

1. Columnar microstructure in both single & double layer TBCs could be achieved.
2. A denser third layer on top of the columnar coatings could be created by spray parameter alterations.
3. Lower thermal conductivity & improved thermal cyclic fatigue life compared to single layer YSZ can be achieved using the multilayered (GZ/YSZ) TBC approach.

Acknowledgements

The authors thank KK foundation, Sweden, for funding this work. Also, authors would like to thank Mr. Kenneth Anderson & Mr. Jonas Olsson for their assistance.

References

[1] D. Stöver and C. Funke, "Directions of the development of thermal barrier coatings in energy applications," *J. Mater. Process. Technol.*, vol. 92–93, pp. 195–202, Aug. 1999.

[2] J. T. DeMasi-Marcin and D. K. Gupta, "Protective coatings in the gas turbine engine," *Surf. Coat. Technol.*, vol. 68–69, pp. 1–9, Dec. 1994.

[3] R. A. Miller, "Thermal barrier coatings for aircraft engines: history and directions," *J. Therm. Spray Technol.*, vol. 6, no. 1, pp. 35–42, Mar. 1997.

[4] A. Cipitria, I. O. Golosnoy, and T. W. Clyne, "A sintering model for plasma-sprayed zirconia TBCs. Part I: Free-standing coatings," *Acta Mater.*, vol. 57, no. 4, pp. 980–992, Feb. 2009.

[5] M. P. Borom, C. A. Johnson, and L. A. Peluso, "Role of environmental deposits and operating surface temperature in spallation of air plasma sprayed thermal barrier coatings," *Surf. Coat. Technol.*, vol. 86–87, no. PART 1, pp. 116–126, 1996.

[6] C. Mercer, S. Faulhaber, A. G. Evans, and R. Darolia, "A delamination mechanism for thermal barrier coatings subject to calcium–magnesium–alumino-silicate (CMAS) infiltration," *Acta Mater.*, vol. 53, no. 4, pp. 1029–1039, Feb. 2005.

[7] J. M. Drexler, C.-H. Chen, A. D. Gledhill, K. Shinoda, S. Sampath, and N. P. Padture, "Plasma sprayed gadolinium zirconate thermal barrier coatings that are resistant to damage by molten Ca–Mg–Al–silicate glass," *Surf. Coat. Technol.*, vol. 206, no. 19–20, pp. 3911–3916, May 2012.

[8] J. Wu, H. Guo, M. Abbas, and S. Gong, "Evaluation of plasma sprayed YSZ thermal barrier coatings with the CMAS deposits infiltration using impedance spectroscopy," *Prog. Nat. Sci. Mater. Int.*, vol. 22, no. 1, pp. 40–47, Feb. 2012.

[9] L. Li, N. Hitchman, and J. Knapp, "Failure of Thermal Barrier Coatings Subjected to CMAS Attack," *J. Therm. Spray Technol.*, vol. 19, no. 1–2, pp. 148–155, Jul. 2009.

[10] J. M. Drexler, K. Shinoda, A. L. Ortiz, D. Li, A. L. Vasiliev, A. D. Gledhill, S. Sampath, and N. P. Padture, "Air-plasma-sprayed thermal barrier coatings that are resistant to high-temperature attack by glassy deposits," *Acta Mater.*, vol. 58, no. 20, pp. 6835–6844, Dec. 2010.

[11] S. Krämer, J. Yang, C. G. Levi, and C. A. Johnson, "Thermochemical Interaction of Thermal Barrier Coatings with Molten CaO–MgO–Al_2O_3–SiO_2 (CMAS) Deposits," *J. Am. Ceram. Soc.*, vol. 89, no. 10, pp. 3167–3175, Oct. 2006.

[12] A. D. Gledhill, K. M. Reddy, J. M. Drexler, K. Shinoda, S. Sampath, and N. P. Padture, "Mitigation of damage from molten fly ash to air-plasma-sprayed thermal barrier coatings," *Mater. Sci. Eng. A*, vol. 528, no. 24, pp. 7214–7221, Sep. 2011.

[13] J. M. Drexler, A. L. Ortiz, and N. P. Padture, "Composition effects of thermal barrier coating ceramics on their interaction with molten Ca–Mg–Al–silicate (CMAS) glass," *Acta Mater.*, vol. 60, no. 15, pp. 5437–5447, Sep. 2012.

[14] B. Saruhan, P. Francois, K. Fritscher, and U. Schulz, "EB-PVD processing of pyrochlore-structured $La_2Zr_2O_7$-based TBCs," *Surf. Coat. Technol.*, vol. 182, no. 2–3, pp. 175–183, Apr. 2004.

[15] D. Stöver, G. Pracht, H. Lehmann, M. Dietrich, J.-E. Döring, and R. Vaßen, "New material concepts for the next generation of plasma-sprayed thermal barrier coatings," *J. Therm. Spray Technol.*, vol. 13, no. 1, pp. 76–83, Mar. 2004.

[16] M. P. Schmitt, A. K. Rai, R. Bhattacharya, D. Zhu, and D. E. Wolfe, "'Multilayer thermal barrier coating (TBC) architectures utilizing rare earth doped YSZ and rare earth pyrochlores,'" *Surf. Coat. Technol.*, vol. 251, pp. 56–63, Jul. 2014.

[17] G. Mauer, D. Sebold, R. Vaßen, and D. Stöver, "Improving Atmospheric Plasma Spraying of Zirconate Thermal Barrier Coatings Based on Particle Diagnostics," *J. Therm. Spray Technol.*, vol. 21, no. 3–4, pp. 363–371, Nov. 2011.
[18] R. Vassen, X. Cao, F. Tietz, D. Basu, and D. Stöver, "Zirconates as New Materials for Thermal Barrier Coatings," *J. Am. Ceram. Soc.*, vol. 83, no. 8, pp. 2023–2028, Aug. 2000.
[19] J. Wu, X. Wei, N. P. Padture, P. G. Klemens, M. Gell, E. García, P. Miranzo, and M. I. Osendi, "Low-Thermal-Conductivity Rare-Earth Zirconates for Potential Thermal-Barrier-Coating Applications," *J. Am. Ceram. Soc.*, vol. 85, no. 12, pp. 3031–3035, Dec. 2002.
[20] Z. Xu, L. He, R. Mu, S. He, and X. Cao, "Preparation and characterization of $La_2Zr_2O_7$ coating with the addition of Y_2O_3 by EB-PVD," *J. Alloys Compd.*, vol. 492, no. 1–2, pp. 701–705, Mar. 2010.
[21] S. V. U. A. V. Radha, "Thermochemistry of lanthanum zirconate pyrochlore," *J. Mater. Res.*, vol. 24, no. 11, pp. 3350 – 3357, 2009.
[22] G. Mauer, M. O. Jarligo, D. E. Mack, and R. Vaßen, "Plasma-Sprayed Thermal Barrier Coatings: New Materials, Processing Issues, and Solutions," *J. Therm. Spray Technol.*, vol. 22, pp. 646–658, Jun. 2013.
[23] S. R. Choi, N. P. Bansal, and D. Zhu, "Mechanical and thermal properties of advanced oxide materials for higher-temperature coatings applications," presented at the Ceramic Engineering and Science Proceedings, 2005, vol. 26, pp. 11–19.
[24] E. Bakan, D. E. Mack, G. Mauer, and R. Vaßen, "Gadolinium Zirconate/YSZ Thermal Barrier Coatings: Plasma Spraying, Microstructure, and Thermal Cycling Behavior," *J. Am. Ceram. Soc.*, vol. 97, no. 12, pp. 4045–4051, Dec. 2014.
[25] X. Zhong, H. Zhao, X. Zhou, C. Liu, L. Wang, F. Shao, K. Yang, S. Tao, and C. Ding, "Thermal shock behavior of toughened gadolinium zirconate/YSZ double-ceramic-layered thermal barrier coating," *J. Alloys Compd.*, vol. 593, pp. 50–55, Apr. 2014.
[26] R. M. Leckie, S. Krämer, M. Rühle, and C. G. Levi, "Thermochemical compatibility between alumina and ZrO_2–$GdO_{3/2}$ thermal barrier coatings," *Acta Mater.*, vol. 53, no. 11, pp. 3281–3292, Jun. 2005.
[27] X. Zhong, H. Zhao, C. Liu, L. Wang, F. Shao, X. Zhou, S. Tao, and C. Ding, "Improvement in thermal shock resistance of gadolinium zirconate coating by addition of nanostructured yttria partially-stabilized zirconia," *Ceram. Int.*, vol. 41, no. 6, pp. 7318–7324, Jul. 2015.
[28] K. S. Lee, D. H. Lee, and T. W. Kim, "Microstructure controls in Gadolinium Zirconate/YSZ double layers and their properties," *J. Ceram. Soc. Jpn.*, vol. 122, no. 1428, pp. 668–673, 2014.
[29] E. Bakan, D. E. Mack, G. Mauer, R. Mücke, and R. Vaßen, "Porosity–Property Relationships of Plasma-Sprayed $Gd_2Zr_2O_7$/YSZ Thermal Barrier Coatings," *J. Am. Ceram. Soc.*, Apr. 2015.
[30] L. Wang, Y. Wang, X. G. Sun, J. Q. He, Z. Y. Pan, and C. H. Wang, "Finite element simulation of residual stress of double-ceramic-layer $La_2Zr_2O_7$/8YSZ thermal barrier coatings using birth and death element technique," *Comput. Mater. Sci.*, vol. 53, no. 1, pp. 117–127, Feb. 2012.
[31] L. Wang, Y. Wang, X. G. Sun, J. Q. He, Z. Y. Pan, and C. H. Wang, "Thermal shock behavior of 8YSZ and double-ceramic-layer $La_2Zr_2O_7$/8YSZ thermal barrier coatings fabricated by atmospheric plasma spraying," *Ceram. Int.*, vol. 38, no. 5, pp. 3595–3606, Jul. 2012.
[32] C. Wang, Y. Wang, L. Wang, G. Hao, X. Sun, F. Shan, and Z. Zou, "Nanocomposite Lanthanum Zirconate Thermal Barrier Coating Deposited by Suspension Plasma Spray Process," *J. Therm. Spray Technol.*, vol. 23, no. 7, pp. 1030–1036, Feb. 2014.
[33] L. Pawlowski, "Suspension and solution thermal spray coatings," *Surf. Coat. Technol.*, vol. 203, no. 19, pp. 2807–2829, Jun. 2009.
[34] R. S. Lima and B. R. Marple, "Nanostructured YSZ thermal barrier coatings engineered to counteract sintering effects," *Mater. Sci. Eng. A*, vol. 485, no. 1–2, pp. 182–193, Jun. 2008.
[35] P. Fauchais, V. Rat, J.-F. Coudert, R. Etchart-Salas, and G. Montavon, "Operating parameters for suspension and solution plasma-spray coatings," *Surf. Coat. Technol.*, vol. 202, no. 18, pp. 4309–4317, Jun. 2008.
[36] K. VanEvery, M. J. M. Krane, R. W. Trice, H. Wang, W. Porter, M. Besser, D. Sordelet, J. Ilavsky, and J. Almer, "Column Formation in Suspension Plasma-Sprayed Coatings and Resultant Thermal Properties," *J. Therm. Spray Technol.*, vol. 20, no. 4, pp. 817–828, Mar. 2011.

[37] N. Curry, K. VanEvery, T. Snyder, and N. Markocsan, "Thermal Conductivity Analysis and Lifetime Testing of Suspension Plasma-Sprayed Thermal Barrier," *Coatings*, vol. 4, no. 3, pp. 630–650, Aug. 2014.
[38] N. Curry, Z. Tang, N. Markocsan, and P. Nylén, "Influence of bond coat surface roughness on the structure of axial suspension plasma spray thermal barrier coatings — Thermal and lifetime performance," *Surf. Coat. Technol.*, vol. 268, pp. 15–23, Apr. 2015.
[39] N. Curry, K. VanEvery, T. Snyder, J. Susnjar, and S. Bjorklund, "Performance Testing of Suspension Plasma Sprayed Thermal Barrier Coatings Produced with Varied Suspension Parameters," *Coatings*, vol. 5, no. 3, pp. 338–356, Jul. 2015.
[40] "ImageJ," *Softonic*. http://imagej.en.softonic.com/.
[41] G. Moskal, L. Swadźba, M. Hetmańczyk, B. Witala, B. Mendala, J. Mendala, and P. Sosnowy, "Characterization of microstructure and thermal properties of $Gd_2Zr_2O_7$-type thermal barrier coating," *J. Eur. Ceram. Soc.*, vol. 32, no. 9, pp. 2025–2034, Jul. 2012.
[42] P. Sokołowski, S. Kozerski, L. Pawłowski, and A. Ambroziak, "The key process parameters influencing formation of columnar microstructure in suspension plasma sprayed zirconia coatings," *Surf. Coat. Technol.*, vol. 260, pp. 97–106, Dec. 2014.
[43] A. Ganvir, N. Curry, S. Björklund, N. Markocsan, and P. Nylén, "Characterization of Microstructure and Thermal Properties of YSZ Coatings Obtained by Axial Suspension Plasma Spraying (ASPS)," *J. Therm. Spray Technol.*, pp. 1–10, Jun. 2015.
[44] X. Q. Cao, R. Vassen, and D. Stoever, "Ceramic materials for thermal barrier coatings," *J. Eur. Ceram. Soc.*, vol. 24, no. 1, pp. 1–10, Jan. 2004.
[45] G. Reisdorf, J. Keller, K. Haltiner, and S. Mukerjee, "Ceramic coatings for insulating modular fuel cell cassettes in a solid-oxide fuel cell stack," Patent US20070134537 A1, Jun-2007.
[46] M. P. van Dijk, A. J. Burggraaf, A. N. Cormack, and C. R. A. Catlow, "Defect structures and migration mechanisms in oxide pyrochlores," *Solid State Ion.*, vol. 17, no. 2, pp. 159–167, Sep. 1985.
[47] M. Pirzada, R. W. Grimes, and J. F. Maguire, "Incorporation of divalent ions in $A_2B_2O_7$ pyrochlores," *Solid State Ion.*, vol. 161, no. 1–2, pp. 81–91, Jul. 2003.
[48] P. J. Wilde and C. R. A. Catlow, "Defects and diffusion in pyrochlore structured oxides," *Solid State Ion.*, vol. 112, no. 3–4, pp. 173–183, Oct. 1998.
[49] P. J. Wilde and C. R. A. Catlow, "Molecular dynamics study of the effect of doping and disorder on diffusion in gadolinium zirconate," *Solid State Ion.*, vol. 112, no. 3–4, pp. 185–195, Oct. 1998.
[50] R. E. Williford, W. J. Weber, R. Devanathan, and J. D. Gale, "Effects of Cation Disorder on Oxygen Vacancy Migration in $Gd_2Ti_2O_7$," *J. Electroceramics*, vol. 3, no. 4, pp. 409–424, Oct. 1999.
[51] L. Minervini, R. W. Grimes, and K. E. Sickafus, "Disorder in Pyrochlore Oxides," *J. Am. Ceram. Soc.*, vol. 83, no. 8, pp. 1873–1878, Aug. 2000.
[52] Van D. M.P, de V. K.J, and B. A.J, "Oxygen ion and mixed conductivity in compounds with the fluorite and pyrochlore structure," *Solid State Ion.*, vol. 9 & 10, pp. 913–920, 1983.
[53] Z. Lu, S.-W. Myoung, Y.-G. Jung, G. Balakrishnan, J. Lee, and U. Paik, "Thermal Fatigue Behavior of Air-Plasma Sprayed Thermal Barrier Coating with Bond Coat Species in Cyclic Thermal Exposure," *Materials*, vol. 6, no. 8, pp. 3387–3403, Aug. 2013.

List of Figures

List of Tables

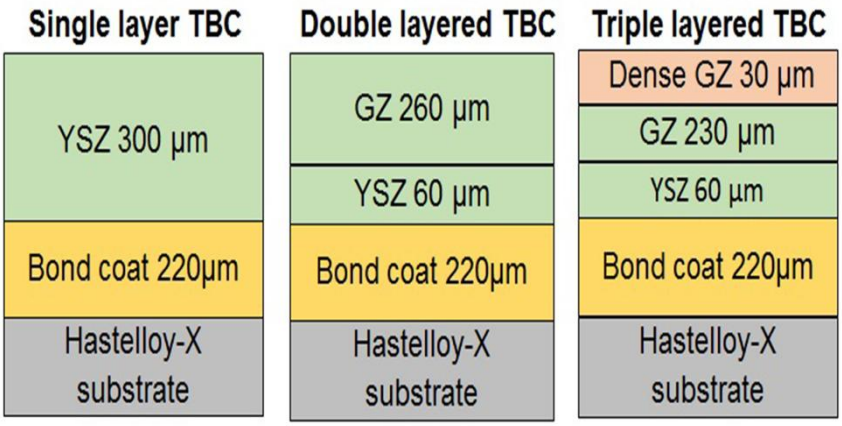

Fig. 1

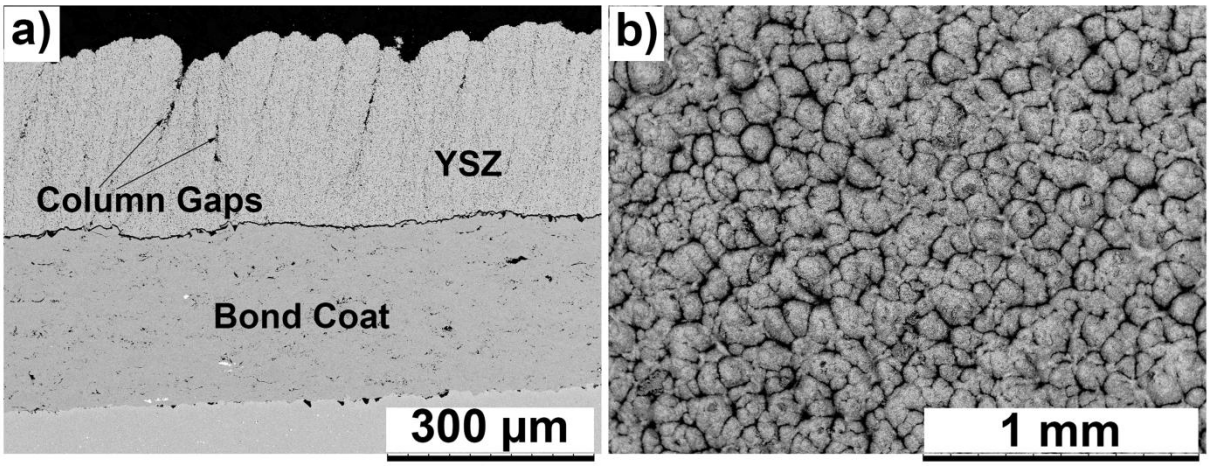

Fig. 2

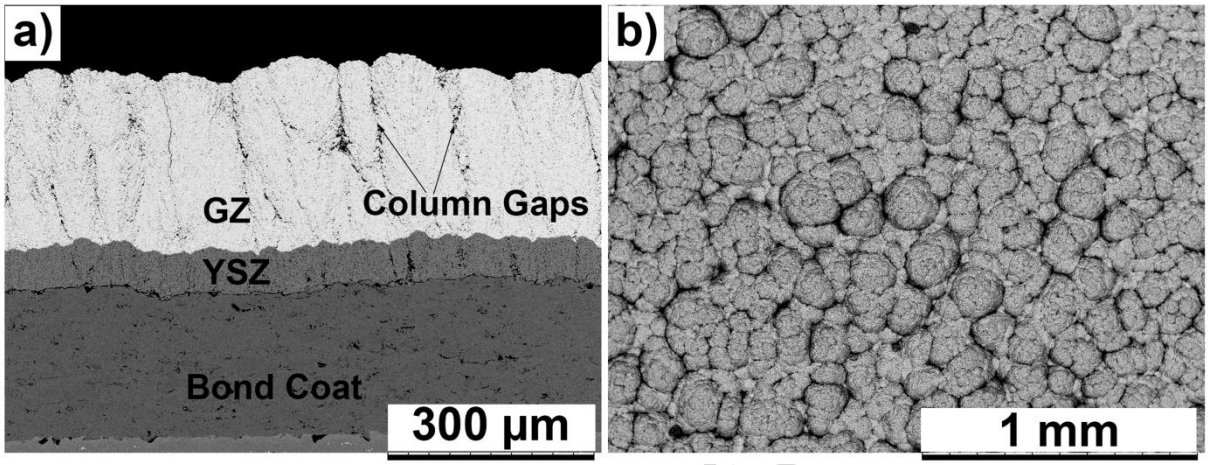

Fig. 3

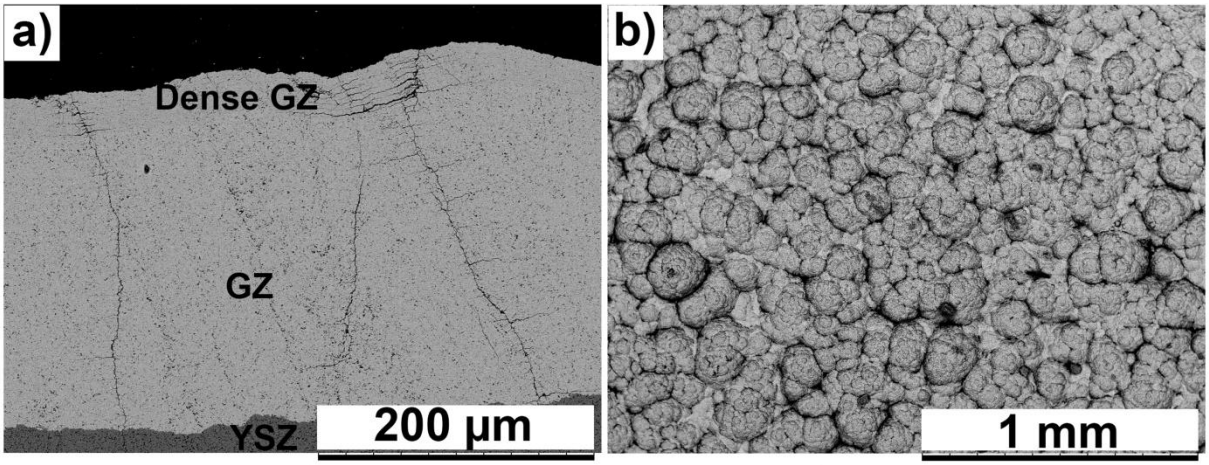

Fig. 4

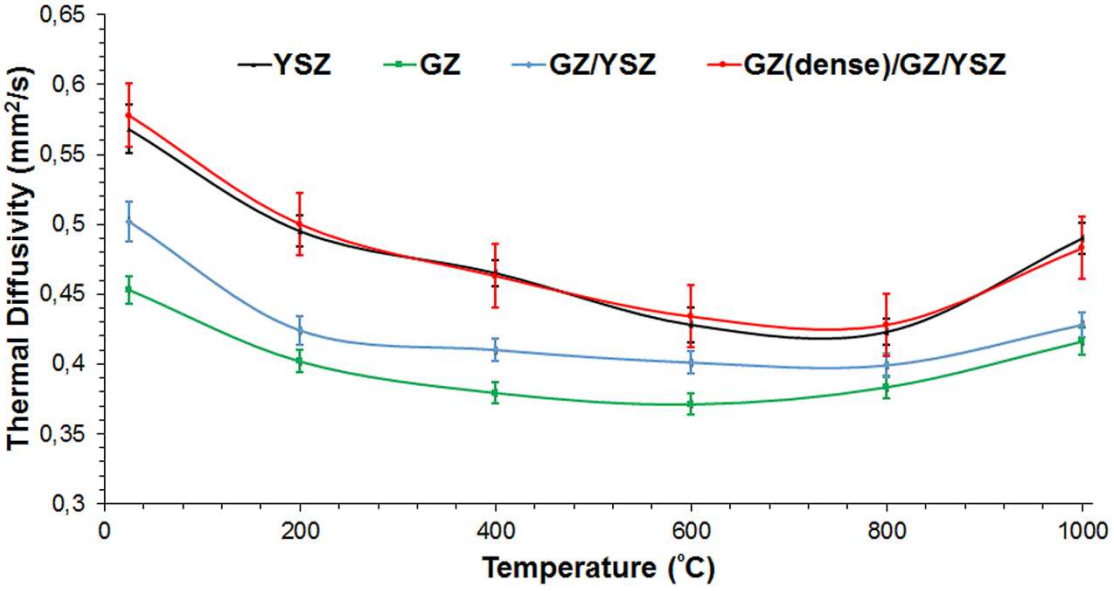

Fig. 5

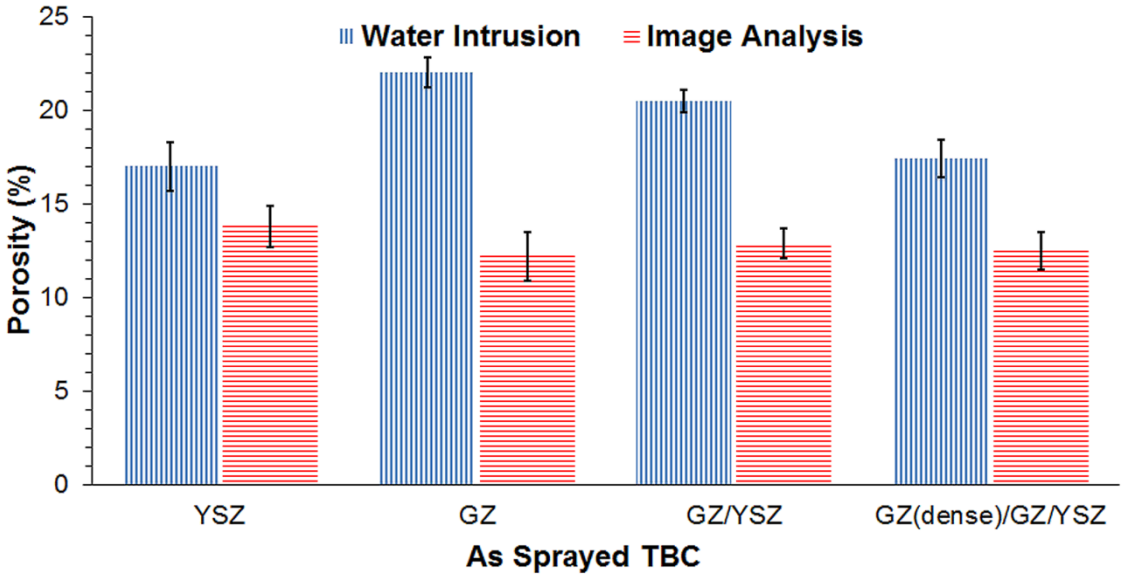

Fig. 6

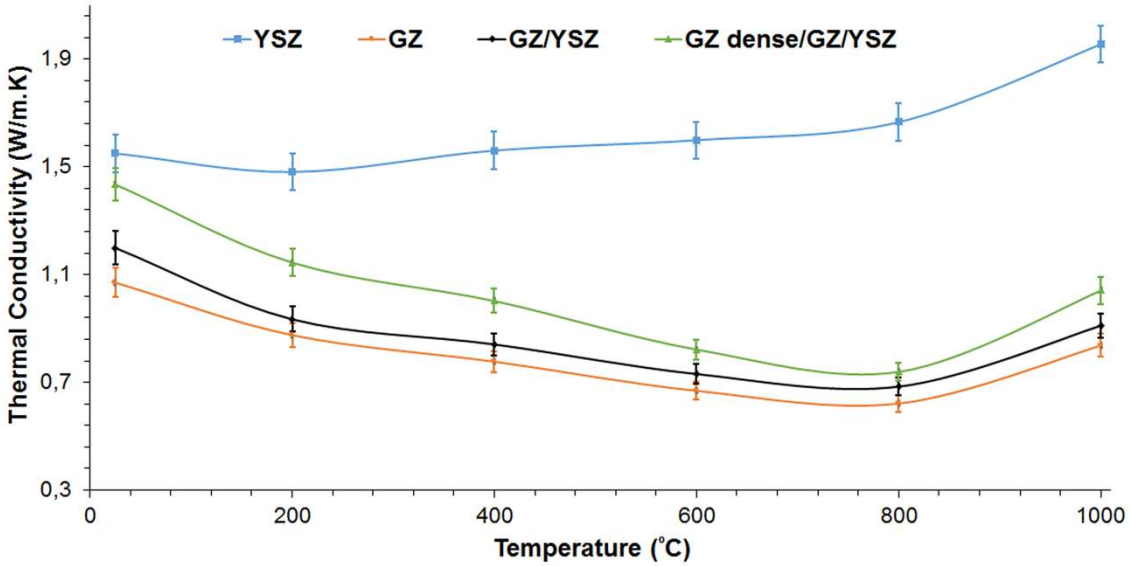

Fig. 7

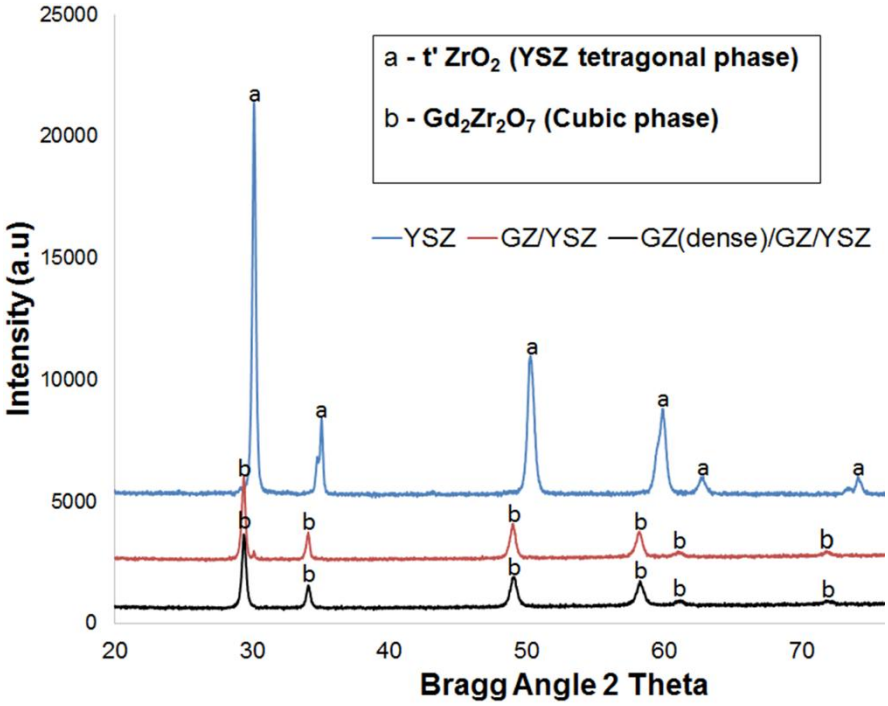

Fig. 8

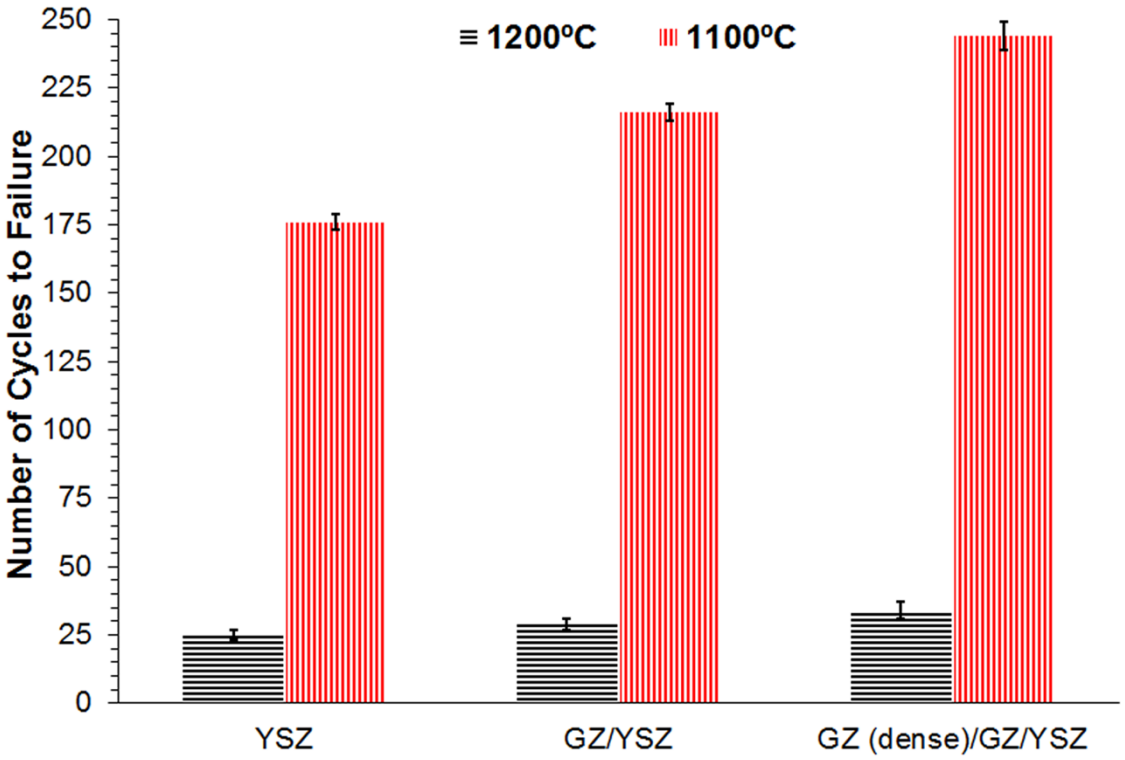

Fig. 9

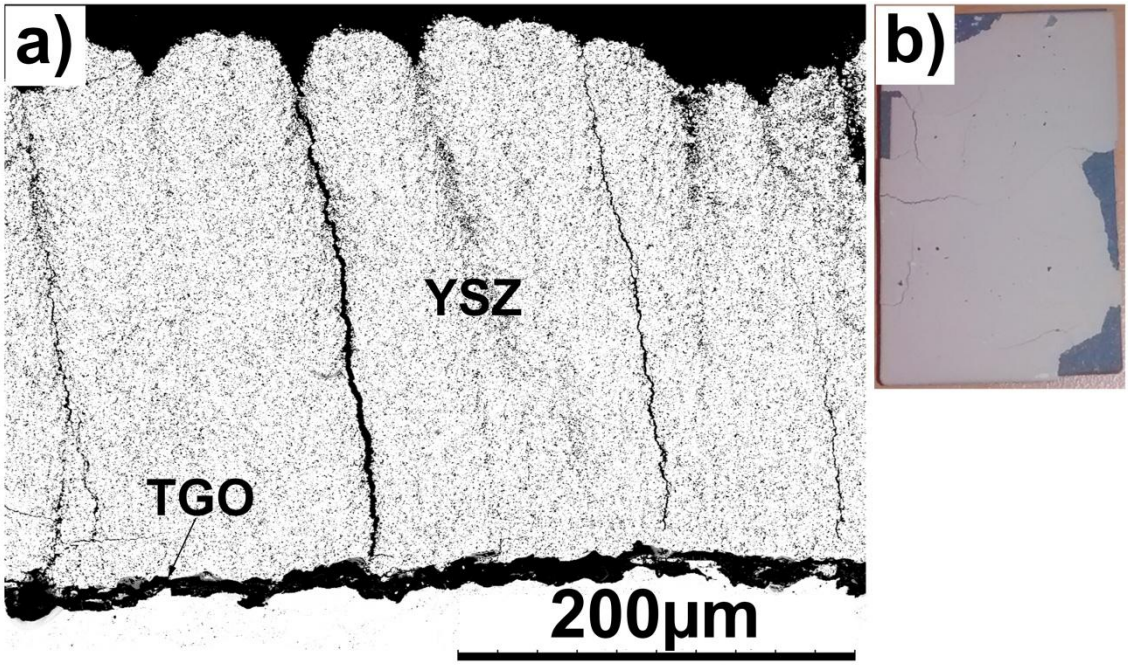

Fig. 10

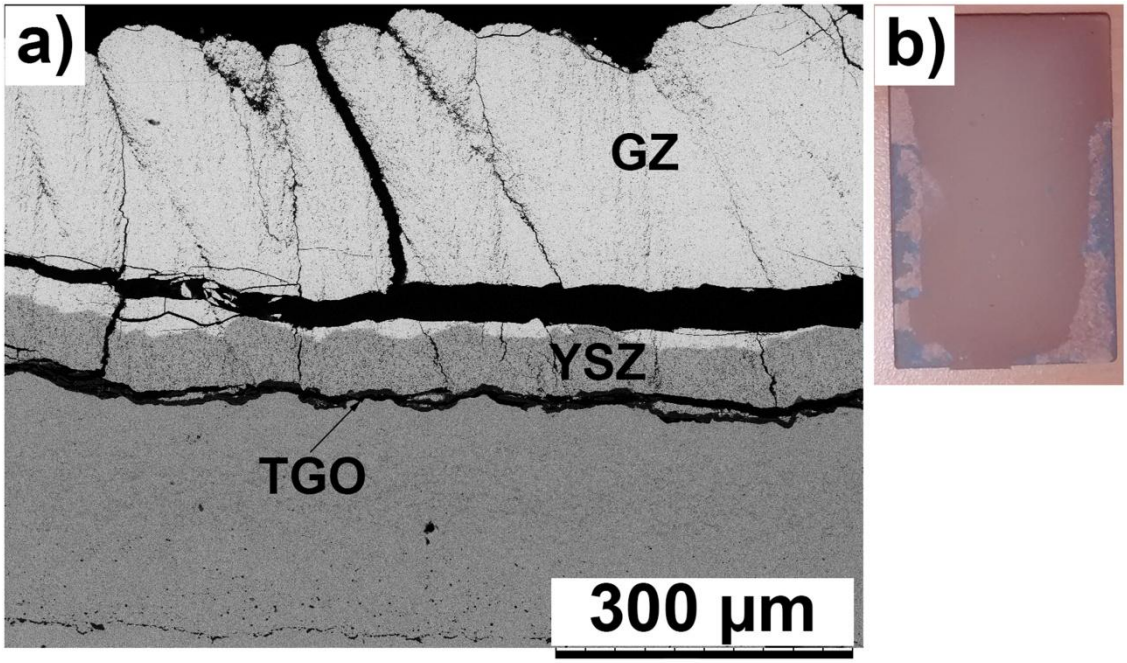

Fig. 11

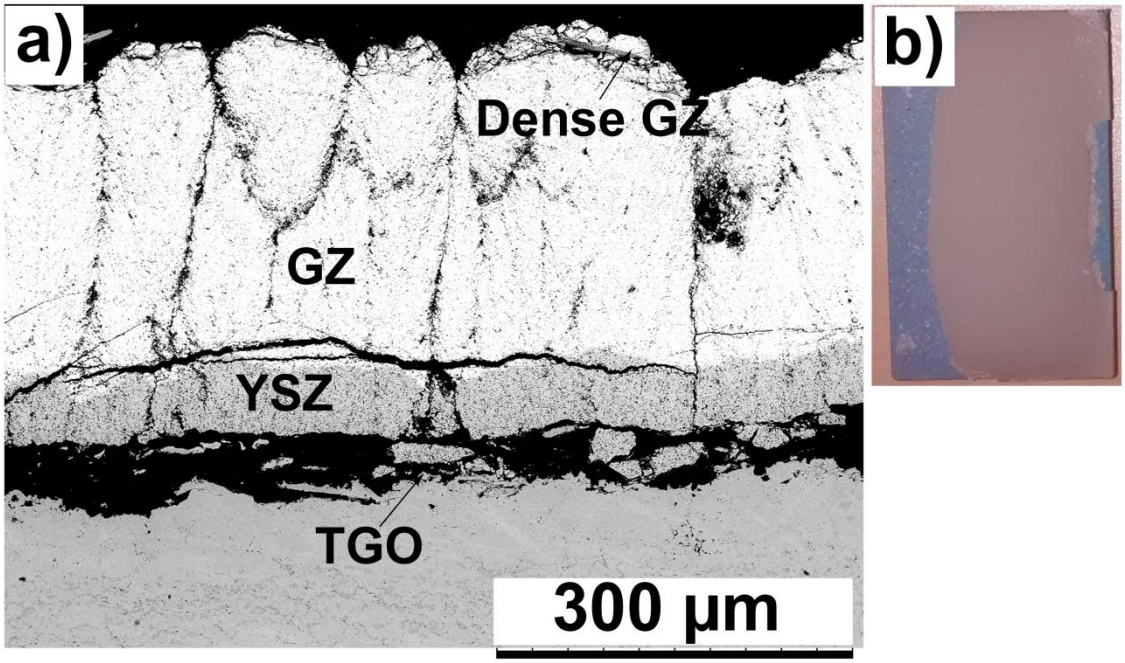

Fig. 12

Table I. Spray parameters used for depositing different layers of single & multilayered TBCs

Parameters	Columnar Layer(s)	Dense Layer
Total Gas Flow	245 l/min	200 l/min
Power	89 kW	103 kW
Jet Enthalpy	7 kJ/l	11 kJ/l
Stand off distance	75 mm	70 mm
Atomizing Gas Flow	20 l/min	5 l/min

Highlights for Review

- The paper titled '**Thermal Conductivity and Thermal Cyclic Fatigue of Multilayered $Gd_2Zr_2O_7$/YSZ Thermal Barrier Coatings Processed by Suspension Plasma Spray**' compares the functional performance of current industry standard 8YSZ thermal barrier coating (TBC) with gadolinium zirchonate/YSZ multilayered TBCs. Novelty of this work is 'suspension plasma spray of GZ/YSZ multilayered TBCs' which has never been reported in the literature to the best of author's knowledge.

Key Findings

- Columnar microstructure in the double layered GZ/YSZ coatings could be achieved.
- A denser top layer in the TBC could be created for CMAS (Calcium Magnesium Alumino Silicates) penetration resistance.
- Lower thermal conductivity TBCs compared to single layer YSZ can be designed using the multilayered approach (GZ/YSZ & GZ dense/GZ/YSZ)
- TBCs with improved thermal cyclic fatigue performance compared to single layer YSZ can be designed using the multilayered approach (GZ/YSZ & GZ dense/GZ/YSZ)